Journal of Physics D: Applied Physics

PAPER • **OPEN ACCESS**

Tunable enhanced Faraday rotation in a defected plasma photonic crystal under external magnetic field with different declinations

To cite this article: Nima Pourali *et al* 2021 *J. Phys. D: Appl. Phys.* **54** 505203

OPEN ACCESS
IOP Publishing
Journal of Physics D: Applied Physics
J. Phys. D: Appl. Phys. **54** (2021) 505203 (9pp)
https://doi.org/10.1088/1361-6463/ac2691

Tunable enhanced Faraday rotation in a defected plasma photonic crystal under external magnetic field with different declinations

Nima Pourali[1,*], Kevon Alexander[1], Volker Hessel[1,2] and Evgeny V Rebrov[1,3,4]

[1] School of Engineering, University of Warwick, Coventry CV4 7AL, United Kingdom
[2] School of Chemical Engineering and Advanced Materials, The University of Adelaide, Adelaide 5005, South Australia, Australia
[3] St. Petersburg State Institute Technology (Technical University), Moskovsky pr. 26, 190013 St. Petersburg, Russia
[4] Department of Chemical Engineering and Chemistry, Eindhoven University of Technology, PO Box 513, 5600 MB Eindhoven, The Netherlands

E-mail: n.pourali86@gmail.com and Nima.Pourali@warwick.ac.uk

Received 19 May 2021, revised 11 August 2021
Accepted for publication 14 September 2021
Published 24 September 2021

Abstract

Magneto-optical responses and the potential for tunability when changing the variables of a one-dimensional defected magnetized plasma photonic crystal have been studied using a transfer matrix method for operation in the mm-range wavelength region. The effect of the number and dielectric defect layer thickness as well as the intensity and declination angle of magnetic field on transmittance, Faraday rotation, and its ellipticity has been investigated. The results demonstrate the ability to alter the resonant modes frequency at multiple levels of precision. The structures with four, six, and eight defect layers have been investigated. The number of defect dielectric layers changes the number of resonance modes. A single defect mode appears within the photonic bandgap with four defect dielectric layers while two defect modes were observed with six layers, and three modes with eight layers. An increase in magnetic field declination decreased the Faraday rotation intensity and width of Faraday resonance mode.

Keywords: photonic crystal, plasma, defect modes, magnetic field declination, Faraday rotation

(Some figures may appear in colour only in the online journal)

1. Introduction

Photonic crystals are artificial periodic structures that consist of alternating layers of materials with different refractive indices. They are designed to restrict a small range of predetermined frequencies of electromagnetic (EM) radiation through the generation of a photonic bandgap. The bandgap is formed as a result of Bragg scattering occurring when EM waves are propagating through the crystal. Since the development of these systems, multiple in-depth studies involving different aspects of the interaction between EM waves and photonic crystals have been analysed [1–6]. The properties of the initial interface layer of the photonic crystal and the formation of surface modes upon it were analysed by Shukla *et al* [7]. Several studies have been conducted involving photonic crystals with

* Author to whom any correspondence should be addressed.

multiple bandgaps, which describe the ability to extend the effective bandgap by overlapping smaller bandgaps to restrict the propagation of a larger range of EM wave frequencies [8–10]. Regarding the structure of the crystal, the consistency in the arrangement of the layers creates periodicity within the structure, and this periodicity is also achieved by alternating the layers in multiple dimensions, for example in two dimensions, which has been previously studied by Sakai *et al* [11]. A 3D photonic crystal allows EM wave propagation in different directions. In combination with the total internal reflection of EM waves, the 3D crystal facilitates complete control over the direction of propagation of certain frequencies, as well as a spatial assortment of EM waves [12]. Defect layers can be introduced into the photonic crystal in between main layers to allow target EM waves of certain frequencies to propagate through the photonic bandgap, whilst rejecting other frequencies [10, 13]. The control of crystal layer structure introduces a method by which the photonic bandgap can be modified to allow specific frequencies of EM waves within the photonic bandgap to be observed. This allows the resulted photonic crystal to be considered as an optical filter.

Magnetophotonic crystals are photonic crystals within an external magnetic field which induces circular polarization (CP) of the EM wave passing through the crystal, in addition to the photonic bandgap generated by the properties of the photonic crystal [14]. If the crystal is composed of materials that have magnetic properties, magneto-optical effects can be manipulated to achieve optimal results. Inoue [15] covers different materials used within multiple layers of the photonic crystal. They also observed multi-dimensional photonic crystals, up to three-dimensional magnetophotonic crystals.

Magneto-optical effects, such as Faraday rotation and Kerr effect, are phenomenon that occur when EM radiation interacts with a magnetic field [16, 17]. For a linearly polarized light source, the wave will experience nonreciprocal rotation if the direction of the magnetic field vector is not parallel to the direction of the magnetic component of propagating EM wave [18]. The direction of this rotation is determined solely by the direction of the magnetic wave, and consequently, the direction of wave propagation does not affect its apparent rotation. Nonreciprocal photonic crystals are used in optical diodes due to their unidirectionality created by magnetisation of crystal layers with magnetic properties [19]. Nishizawa *et al* stated that a 3D magnetophotonic crystal within which light propagates perpendicularly to the direction of external magnetic field vector experiences a band Faraday effect which has been described as a unique phenomenon [15, 20]. Khanikaev *et al* [21] built a 2D model of a magnetophotonic crystal. They showed that under the condition of Faraday geometry the magnetic field eliminates any degeneracy in the photonic band structure and optical activity reduces the symmetry of the system.

However, in the magnetophotonic crystal structures the dielectric layer properties such as their refractive index are fixed, therefore the frequency of the EM wave that they permit is also fixed. To tune the frequency, plasma layers with variable parameters can be introduced, forming plasma photonic crystals [22–26]. In these crystals, the properties of plasma layers can be adjusted by an external magnetic field. The direction and orientation of the magnetic field contributes towards the arrangement of the plasma layers, directly affecting the frequencies of light that can pass through the photonic bandgap. Therefore, these magnetophotonic crystals allow for the greatest amount of photonic bandgap modification. Application of plasma layers allows for the generation of more dynamic photonic crystals with an increased number of practical applications such as plasma lens, plasma antenna, plasma stealth aircraft, etc [27–29]. The study of EM waves propagating through photonic crystals under magnetic field with nonzero declination angle has been limited to the magnitudes of transmittance and reflectance for any incident wave onto the crystal, as shown by Zhang *et al* [30] and Qi *et al* [31]. Reflection properties for a 1D plasma photonic crystal have been extensively studied by Kumar *et al*, who proposed a relationship between the plasma layer thickness and the photonic bandgap [32]. Mehdian *et al* [33] observed the Faraday effect for the same plasma photonic crystal.

Based on the finding in recent magneto-optical crystal structures, a detailed mechanism for the EM wave interaction with a 1D magnetic plasma photonic crystal considering magnetic field declination can be developed, which would allow controlling the underlying phenomena with great degrees of precision. Kahl and Grishin suggested that these phenomena can be optimised by making use of resonance for 1D magneto-photonic crystals [34]. This could lead to a plethora of industrial applications and has the potential to affect current optics technology, due to the wide range of use of 1D photonic crystals that are currently available in the communication and optics industries. However, the influence of magnetic field declination angle and the presence of defect layers in the plasma photonic crystals on their magneto-optical properties have not been reported.

This report intends to explore the magneto-optical effects exhibited by EM waves that propagate through photonic crystals that are under varying degrees of magnetic field declination. To this end, a 4 by 4 transfer matrix method is employed to study the magneto-optical effects in a plasma photonic crystal, defected by a dielectric layer, under an external magnetic field with different declination angles. The procedure and the description of the model are presented in the next section. In section 3, the results of the study are discussed and the last section is devoted to summarising the main finding of the work.

2. Model and theory

Figure 1 shows a schematic view of the structure of the photonic crystal to be studied in this paper. The crystal layers are parallel with the *xy* plane, as the periodicity of the structure is along the *z*-direction. This model has the m layers of dielectric (D) in the middle which are surrounded with s composite layers (AP and PA) of dielectric (A) and plasma (P). The structure will be referred to as follows: $(AP)^s(D)^m(PA)^s$. Dielectric

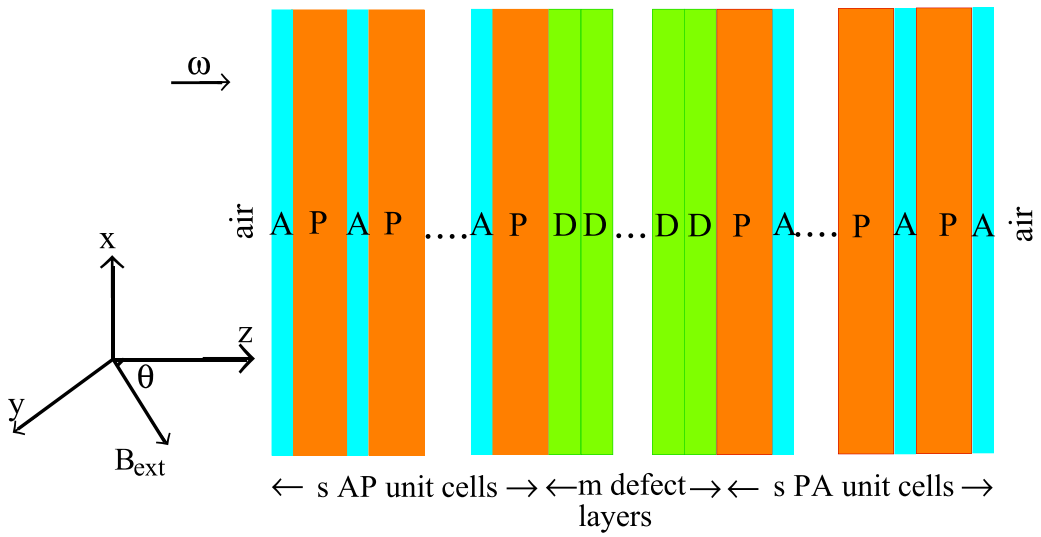

Figure 1. Schematic structure of the defected plasma photonic crystal having the arrangement $(AP)^s(D)^m(PA)^s$.

layers A and D are BaF_2 and ZnSe respectively with refractive indices of $N_A = 1.4$ and $N_D = 2.4$. The design wavelength (λ_0) is assumed to be 10 mm. Thickness of plasma layer is fixed to $\lambda_0/4 = 2.5$ mm and the thickness of dielectric layers is determined by $d_A = \lambda_0/4N_D = 1.78$ mm and $d_D = \lambda_0/4N_A = 1.04$ mm. Also, it is assumed that layers are indefinitely large, although it is not important when wave is shined in normal to layer on a 1-D photonic crystal. The behaviour of the plasma layers in a static magnetic field with the direction vector normal to the dielectric layers (shown in figure 1, when azimuth angle (θ) is equal to 0°) are described in their permittivity tensor as:

$$\varepsilon_p = \begin{pmatrix} \varepsilon_{xx}(\omega) & \varepsilon_{xy}(\omega) & 0 \\ -\varepsilon_{yx}(\omega) & \varepsilon_{yy}(\omega) & 0 \\ 0 & 0 & \varepsilon_{zz}(\omega) \end{pmatrix}, \tag{1}$$

within which,

$$\varepsilon_{xx}(\omega) = \varepsilon_0 \left[1 - \frac{\omega_p(\omega + i\vartheta_c)}{\omega\left[(\omega + i\vartheta_c)^2 - \omega_c^2\right]} \right] \tag{2}$$

$$\varepsilon_{xy}(\omega) = \varepsilon_{yx}(\omega) = \frac{-i\varepsilon_0\omega_p^2\omega_c}{\omega\left[(\omega + i\vartheta_c)^2 - \omega_c^2\right]} \tag{3}$$

$$\varepsilon_{zz}(\omega) = \varepsilon_0 \left[1 - \frac{{\omega_p}^2}{\omega(\omega + i\vartheta_c)} \right] \tag{4}$$

where ϑ_c represents the plasma collision frequency, $\omega_p = (e^2 n_e/\varepsilon_0 m_e)^{1/2}$ denotes the electron plasma frequency, $\omega_c = (eB/m_e)$ denotes plasma cyclotron frequency with B being magnetic field intensity, ε_0 represents dielectric constant in vacuum, m_e equals electron mass, e is electron charge, and n_e represents plasma density. To study the effect of magnetic field declination angle, a adapted permittivity tensor must be introduced to account for changes to the magnetic field direction. By following approach presented in [30], the generalized permittivity tensor is given by

$$\varepsilon'_P = T \begin{pmatrix} \varepsilon_{xx}(\omega) & \varepsilon_{xy}(\omega) & 0 \\ -\varepsilon_{yx}(\omega) & \varepsilon_{yy}(\omega) & 0 \\ 0 & 0 & \varepsilon_{zz}(\omega) \end{pmatrix} T^{-1} \tag{5}$$

within which,

$$T = \begin{pmatrix} 0 & 1 & 0 \\ -\cos(\theta) & 0 & \sin(\theta) \\ \sin(\theta) & 0 & \cos(\theta) \end{pmatrix}, \quad T^{-1} = \begin{pmatrix} 0 & -\cos(\theta) & \sin(\theta) \\ 1 & 0 & 0 \\ 0 & \sin(\theta) & \cos(\theta) \end{pmatrix}, \tag{6}$$

where use of T and T^{-1} simply represents the effect of changing the angle has on the initial permittivity tensor. A combination of equations (5) and (6) results in equation (7):

$$\varepsilon'_P = \begin{pmatrix} \varepsilon_{yy}(\omega) & \varepsilon_{xy}(\omega)\cos(\theta) & -\varepsilon_{xy}(\omega)\sin(\theta) \\ -\varepsilon_{xy}(\omega)\cos(\theta) & \varepsilon_{xx}(\omega)\cos^2(\theta) + \varepsilon_{zz}(\omega)\sin^2(\theta) & (\varepsilon_{zz}(\omega) - \varepsilon_{xx}(\omega))\sin(\theta)\cos(\theta) \\ \varepsilon_{xy}(\omega)\sin(\theta) & (\varepsilon_{zz}(\omega) - \varepsilon_{xx}(\omega))\sin(\theta)\cos(\theta) & \varepsilon_{xx}(\omega)\sin^2(\theta) + \varepsilon_{zz}(\omega)\cos^2(\theta) \end{pmatrix}. \tag{7}$$

The dielectric layers are not perceived to experience any considerable change as the angle of orientation of the external magnetic field is changing. As a result, the permittivity tensor used to model dielectric layers remains the same as when the field is oriented at normal incidence (equation (8)). Therefore, it can be used for any value of magnetic field declination.

$$\varepsilon_{Di}^{'} = \varepsilon_{Di} = \begin{pmatrix} \varepsilon_d & 0 & 0 \\ 0 & \varepsilon_d & 0 \\ 0 & 0 & \varepsilon_d \end{pmatrix}, \tag{8}$$

where ε_d is the permittivity of the dielectric layer.

Having permittivity tensors, it is possible to apply Maxwell equations inside each jth layer to determine the effective refraction index for each layer in the structure. To this purpose, we assume that the wave vector is parallel to the +z axis ($\vec{K} = \hat{z}k_z = \hat{z}N\omega/c$) and the external magnetic field (B) is along the yz plane and has an arbitrary angle θ with the +z axis. Therefore, the wave equation gives:

$$\begin{bmatrix} N_{(j)}^2 - \varepsilon_{11,(j)} & -\varepsilon_{12,(j)} & -\varepsilon_{13,(j)} \\ -\varepsilon_{21,(j)} & N_{(j)}^2 - \varepsilon_{22,(j)} & -\varepsilon_{23,(j)} \\ -\varepsilon_{31,(j)} & -\varepsilon_{32,(j)} & -\varepsilon_{33,(j)} \end{bmatrix} \begin{bmatrix} E_{0x,(j)} \\ E_{0y,(j)} \\ E_{0z,(j)} \end{bmatrix} = 0, \tag{9}$$

where $\varepsilon_{mn,(j)}$ is the element positioned in row m and column n of permittivity tensor of layer j (see equations (7) and (8)). Also, $E_{0x,(j)}$, $E_{0y,(j)}$, and $E_{0z,(j)}$ are the Cartesian components of the complex electric field amplitude. The determinant of coefficient matrix in equation (9) gives:

$$N_{(j)}^2 = 1 - \frac{\left(\frac{\omega_p}{\omega}\right)^2}{\left[1 + i\frac{\vartheta_c}{\omega} - \frac{\left(\frac{\omega_c}{\omega}\sin(\theta)\right)^2}{2\left(1+i\frac{\vartheta_c}{\omega} - \frac{\omega_p^2}{\omega^2}\right)}\right] \pm \sqrt{\frac{\left(\frac{\omega_c}{\omega}\sin(\theta)\right)^4}{4\left(1+i\frac{\vartheta_c}{\omega} - \frac{\omega_p^2}{\omega^2}\right)^2} + \left(\frac{\omega_c}{\omega}\cos(\theta)\right)^2}}, \tag{10}$$

for plasma layers and

$$N_{(j)}^2 = \varepsilon_{Di}, \tag{11}$$

for dielectric layers. The constant reflective indices of dielectric layers are $N_A = 1.4$ and $N_D = 2.4$. The four eigenvalues given by equation (10) are related to the eigenmodes corresponded to the waves travelling in the forward and backward directions with right- and left-handed circular polarisation. The electric field distribution inside each layer of the structure can be expressed as below:

$$\begin{aligned} \mathbf{E}^{(j)} = \frac{1}{\sqrt{2}}\{ & E_{01}^{(j)}(\hat{X} + i\hat{Y})\exp[-i\frac{\omega}{c}N_+^{(j)}(z - z_j)] \\ & + E_{02}^{(j)}(\hat{X} + i\hat{Y})\exp[i\frac{\omega}{c}N_+^{(j)}(z - z_j)] \\ & + E_{03}^{(j)}(\hat{X} - i\hat{Y})\exp[-i\frac{\omega}{c}N_-^{(j)}(z - z_j)] \\ & + E_{04}^{(j)}(\hat{X} - i\hat{Y})\exp[i\frac{\omega}{c}N_-^{(j)}(z - z_j)]\}, \end{aligned} \tag{12}$$

where jth layer of the structure is extended from interface plane $z = z_{j-1}$ to $z = z_j$ ($z_{j-1} < z_j$) and $E_{01}^{(j)}$ and $E_{02}^{(j)}$ are complex amplitudes of right-hand circular polarized eigen modes propagating, respectively, along positive and negative directions of z-axis at $z = z_j$ while $E_{03}^{(j)}$ and $E_{04}^{(j)}$ denote to corresponding left-hand circular polarized eigen modes. Each distinct layer of the structure is characterized by its dielectric permittivity tensor and the thickness. Following the approach presented in [35], boundary conditions at the interface planes can relate the amplitudes of electric fields in two adjunct layers to each other, resulting:

$$D^{(j-1)}\mathbf{E}_0^{(j-1)} = D^{(j)}P^{(j)}\mathbf{E}_0^{(j)}, \tag{13}$$

where dynamical and propagation matrices, $D^{(j)}$ and $P^{(j)}$, are defined by:

$$D^{(j)} = \begin{bmatrix} 1 & 1 & 0 & 0 \\ N_+^{(j)} & -N_+^{(j)} & 0 & 0 \\ 0 & 0 & 1 & 1 \\ 0 & 0 & N_-^{(j)} & -N_-^{(j)} \end{bmatrix}, \tag{14}$$

and

$$P_j = \begin{bmatrix} \exp(+i\beta_+^{(j)}) & 0 & 0 & 0 \\ 0 & \exp(-i\beta_+^{(j)}) & 0 & 0 \\ 0 & 0 & \exp(+i\beta_-^{(j)}) & 0 \\ 0 & 0 & 0 & \exp(-i\beta_-^{(j)}) \end{bmatrix}. \tag{15}$$

Here $\beta_\pm^{(j)} = \frac{\omega}{c}N_\pm^{(j)}d_j$, with d_j and ω being respectively the thickness of jth layer and angular frequency of incident wave. By using relation (13) and doing mathematical simplifications, the total transfer matrix (M) is obtained to specify the total transmitted and reflected waves of the structure as below:

$$\begin{bmatrix} E_+^i \\ E_+^r \\ E_-^i \\ E_-^r \end{bmatrix} = \begin{bmatrix} M_{11} & M_{12} & 0 & 0 \\ M_{21} & M_{22} & 0 & 0 \\ 0 & 0 & M_{33} & M_{34} \\ 0 & 0 & M_{43} & M_{44} \end{bmatrix} \begin{bmatrix} E_+^t \\ 0 \\ E_-^t \\ 0 \end{bmatrix} \tag{16}$$

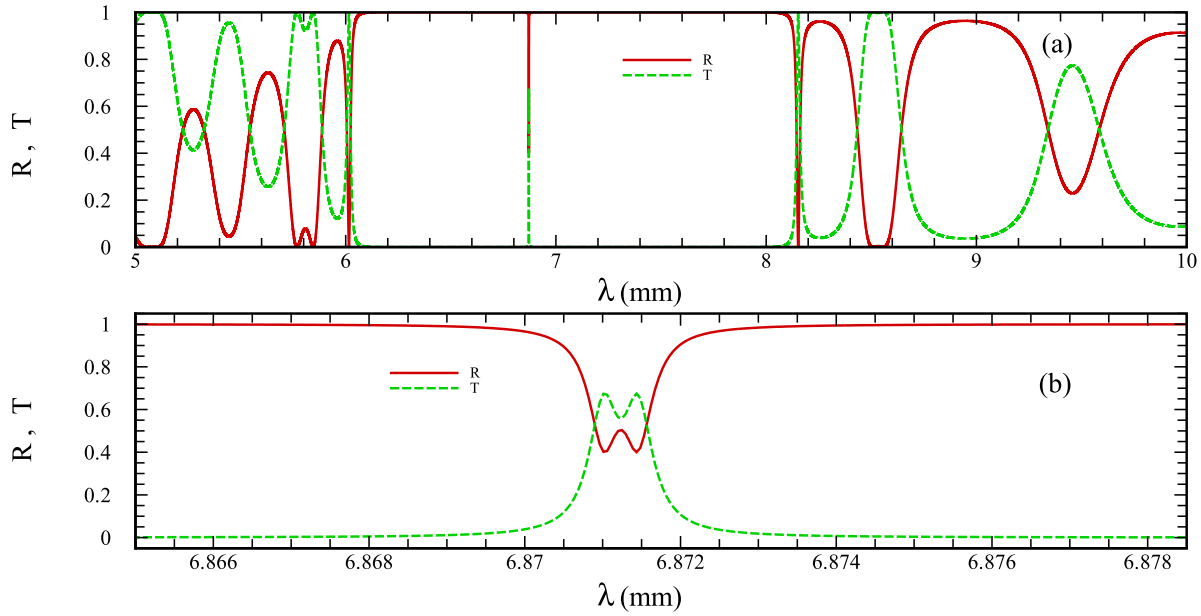

Figure 2. The transmittance and reflectance of structure with repetition numbers $m = 4$ and $s = 6$ at $n_e = 1 \times 10^{+19}$ m^{-3}, $\vartheta_c = (1 \times 10^{-3})\omega_p$, $B = 0.002$ T, and $\theta = 30°$. The bottom figure presents a magnification in defect mode area.

$$M = \left[D^0\right]^{-1} \left(\prod_{j=1}^{J} S^{(j)}\right) D^{(J+1)}, \tag{17}$$

where J is the total number of layers, labels i, r, and t denote to the incident, reflected, and transmitted CP field amplitudes and $S^{(l)}$ matric is given by:

$$S^{(j)} = \begin{bmatrix} \cos\beta_+^{(j)} & \frac{i}{N_+^{(l)}}\sin\beta_+^{(j)} & 0 & 0 \\ iN_+^{(j)}\sin\beta_+^{(l)} & \cos\beta_+^{(j)} & 0 & 0 \\ 0 & 0 & \cos\beta_-^{(j)} & \frac{i}{N_-^{(j)}}\sin\beta_-^{(j)} \\ 0 & 0 & iN_-^{(j)}\sin\beta_-^{(j)} & \cos\beta_-^{(j)} \end{bmatrix}. \tag{18}$$

Having elements of the total transfer matrix, the magneto-optical characteristics of the structure can be calculated too. The complex transmission and reflection coefficients of the right- and left-handed circular polarized waves are determined by arrays of the total transfer matrix as: $t_+ = (M_{11})^{-1}$, $t_- = (M_{33})^{-1}$, $r_+ = (M_{21}/M_{11})$, and $r_- = (M_{43}/M_{33})$. The observable transmittance (T) and reflectance (R) of the structure are determined by the right- and left-handed CP coefficients as follows:

$$T = \frac{1}{2}\left(\left|t_+^2\right| + \left|t_-^2\right|\right), \tag{19}$$

$$R = \frac{1}{2}\left(\left|r_+^2\right| + \left|r_-^2\right|\right). \tag{20}$$

In addition, Faraday rotation (θ_f) and its ellipticity (ξ_k and ξ_f) are calculated as [35]:

$$\theta_f = \frac{1}{2}\arg(\xi_f), \tag{21}$$

$$\tan(\chi_f) = \frac{|\xi_f| - 1}{|\xi_f| + 1}, \tag{22}$$

where $\xi_f = \frac{M_{33}}{M_{11}}$.

3. Numerical results and discussion

This part presents and discusses the results yielded from simulation of the photonic crystal's magneto-optical effects for the proposed structure $(AP)^s D^m (PA)^s$ at the design wavelength, $\lambda_0 = 10$ mm. Fixed parameters for this study were the thickness and the refractive index of dielectric layers, whilst the unit cell number for photonic crystal structure, the magnetic field intensity, and its declination angle were varied.

Figure 2 displays the transmittance (T) and reflectance (R) exhibited by the plasma photonic crystal with repetition numbers of $m = 4$ and $s = 6$. The transmittance and reflectance patterns presented follow relation $R = 1 - T$, as expected. There is a single defect mode present within the photonic bandgap that splits up into two symmetrical peaks. These can be seen at a larger magnification in figure 2(b). For defect mode at the resonant frequency, the reflectance was reduced whilst the transmittance was amplified, demonstrating the unidirectional property of the magnetised plasma photonic crystal.

Figure 3 displays the reflectance and transmittance patterns observed for three different photonic crystals, with different numbers of defect layer (D) . The plot presents the magnitude of the EM wave propagating through the crystal as a function of normalised wave frequency. It can be seen that three defect modes appear for the crystal structure with $m = 8$, whereas two defect modes are seen within the bandgap region at $m = 6$. The two peaks have converged at a central normalised frequency at $m = 4$. There is an overlap in the

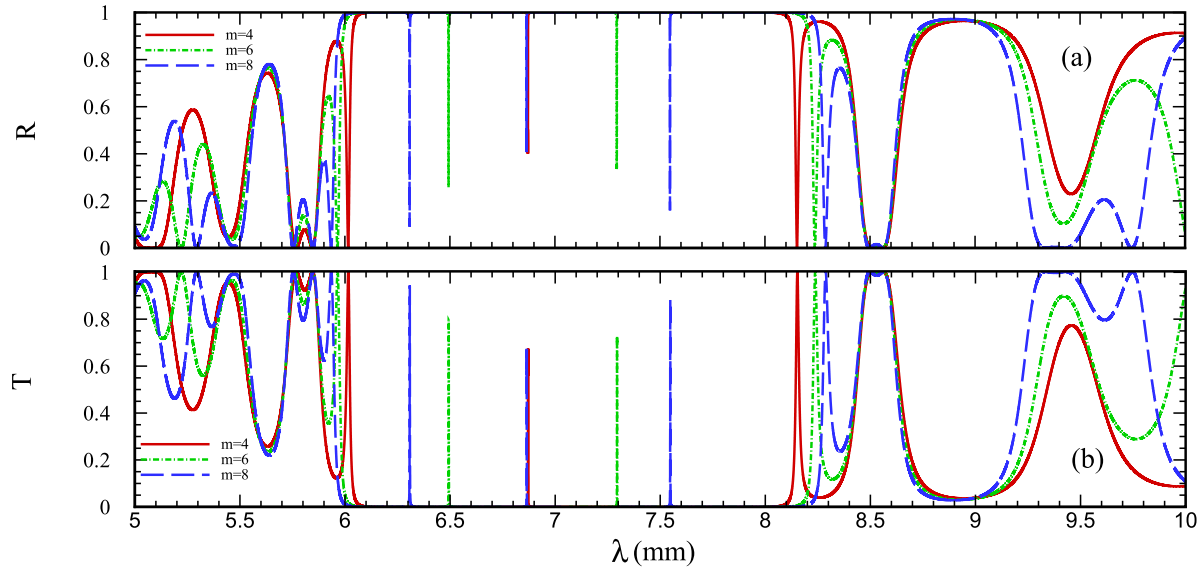

Figure 3. (a) The transmittance (a) and reflectance (b) of structures with different thicknesses for defect layer $m = 4$ (solid), $m = 6$ (dashed-dotted), $m = 8$ (dashed) and same repetition number for surrounding unit cells $s = 6$. The considered parameters are same as figure 2.

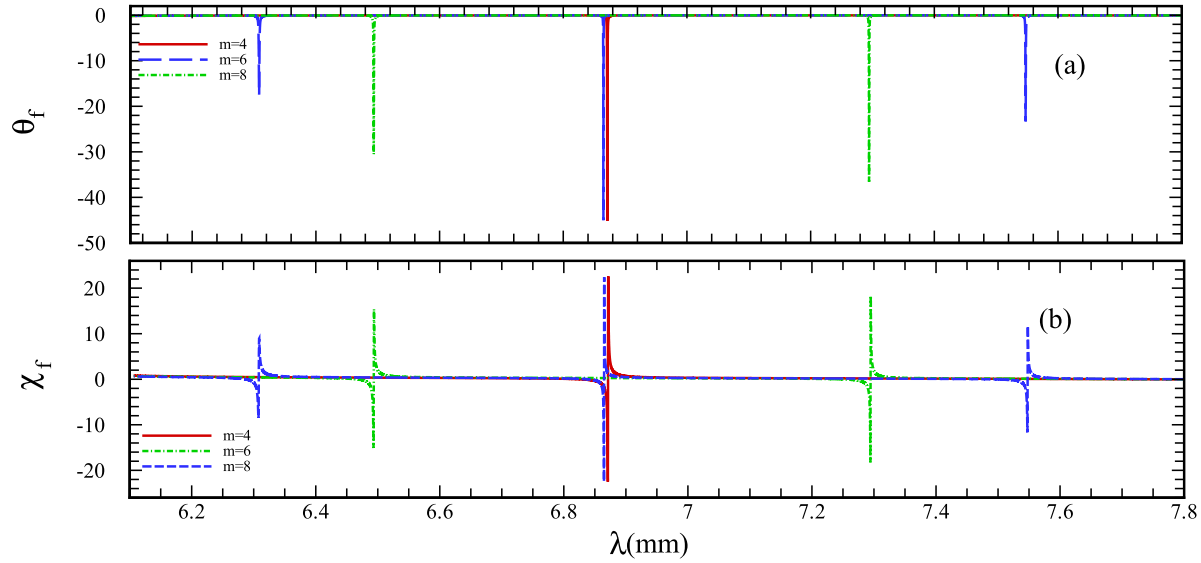

Figure 4. Faraday rotation angle (a) and ellipticity of transmitted wave (b). The conditions are the same as those presented in figure 3.

centre of the photonic bandgap in the defect modes for $m = 4$ and $m = 8$. These modes have also the same magnitude. As the modes move closer to the centre of photonic bandgap, their magnitude decreases for all m values.

Figure 4 shows the Faraday rotation (θ_f) and ellipticity (χ_f) for each photonic crystal as a function of incident wave frequency. The peaks are present at the same frequency as those for transmittance and reflectance of the EM wave in figure 3. As the number of D-layers increases, the distance between the rotation and ellipticity peaks increases for each crystal. For $m = 4$, only one peak was observed for the photonic bandgap, and this peak demonstrates the largest magnitude for both Faraday rotation and ellipticity. As peaks move further apart, their magnitude also decreases. For $m = 8$, three peaks are observed for both Faraday rotation and ellipticity.

The generated resonance mode within the proposed photonic crystal allows the Faraday rotation and ellipticity effects to be studied. It can be seen in figure 5, an increase in the magnetic field strength has resulted in suppression of the transmittance peaks, shown by the decrease in the magnitude of the peaks at the magnetic field of 0.01 T against the peak at the magnetic field of 0.002 T. A notable effect is that the peak for $B = 0.002$ T splits into two smaller peaks and this process continues as the intensity of magnetic field increases. At $B = 0.02$ T two fully separated peaks appear with a larger distance between them. The highest magnetic field gave the highest values of θ_f and χ_f parameters. The shape of the θ_f

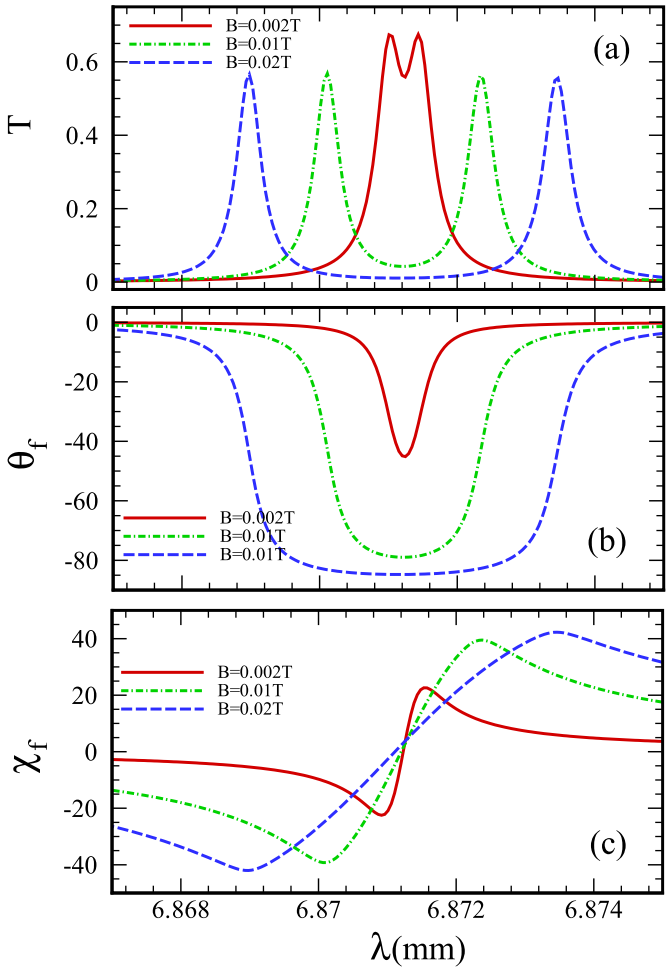

Figure 5. The transmittance (a), Faraday rotation angle (b), ellipticity of transmitted wave (c) for the photonic crystal with $m = 4$ and $s = 6$ under magnetic field with different intensities $B = 0.002\ T$ (solid), $B = 0.01\ T$ (dash-dotted), $B = 0.02\ T$ (dashed). The other parameters are same as figure 2.

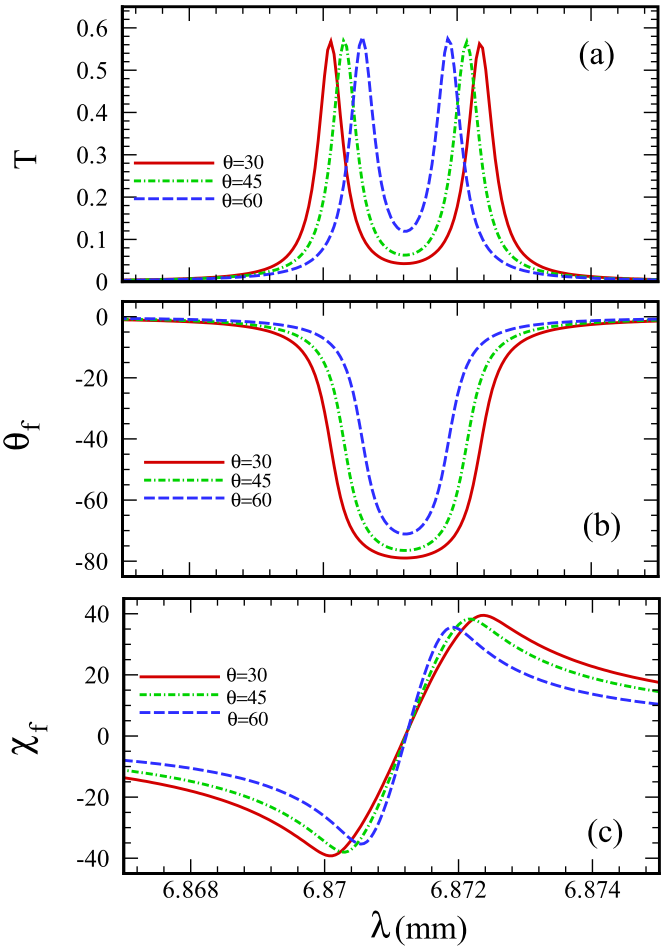

Figure 6. The transmittance (a), Faraday rotation angle (b), ellipticity of transmitted wave (c), for photonic crystal with $m = 4$ and $s = 6$ at three different values of magnetic field declinations: $\theta = 30°$ (solid), $\theta = 45°$ (dash-dotted), and $\theta = 60°$ (dashed) and $B = 0.01\ T$. The other parameters are same as figure 2.

peak becomes wider with the increase in magnetic field magnitude. The ellipticity also reaches larger values at lower frequency as compared with that at week magnetic fields.

As the intended focus of this study is to observe the magneto-optical effects that arise as a result of varying the declination of the external magnetic field encompassing the plasma photonic crystal, the declination angle must be altered and consequent outcomes observed. Figure 6 illustrates transmittance, Faraday rotation, and Faraday ellipticity observed when magnetic field declination angle is oriented at 30°, 45° and 60° degrees. It demonstrates that the location of the defect modes relative to the photonic bandgap can be altered by declination angle, with virtually no loss in magnitude. When the magnetic field declination decreases the Faraday rotation increases and also it experiences longer periods with the magnitude of rotation close to the peak rotation values, over a larger range of normalised wave frequencies. Indeed, Faraday rotation remain close to $-80°$ for the $\theta = 30°$ in a wider frequency range. Also, an increase in declination angle from $\theta = 45°$ to $\theta = 60°$ decreases the magnitude of rotation from $-75°$ to $-70°$. In the case of ellipticity, an increase in declination angle decreases the amplitude of ellipticity and its change is restricted to a small frequency range. The relationship between the magnetic field declination changes being so large in terms of degrees resulting in such small changes in resonant frequencies suggests that tunability with a precision of roughly up to 3.33×10^{-6} per degree can be achieved if the magnetic declination can be varied by units of 1°.

Finally, the last figure (figure 7) shows the transmittance and Faraday rotation for structures with different defect layers, without defect layers, and having different repetition numbers of surrendering unit cells. In figures 7(a) and (b) the transmittance and Faraday rotation for two structures having different defect layers are compared. They show that resonance mode occurs at a bigger wavelength when the defect layer has a smaller reflective index. Also, Faraday rotation is smaller for a structure having a defect layer with a smaller reflective index. Figures 7(c) and (d) show how transmittance and Faraday rotation are affected by removing the defect layers. They show that position of the main resonance changes when the defect layer is removed from the structure. It is noteworthy to mention that after removing the main defect layer (D dielectric layer) the structure is still defective because two plasma

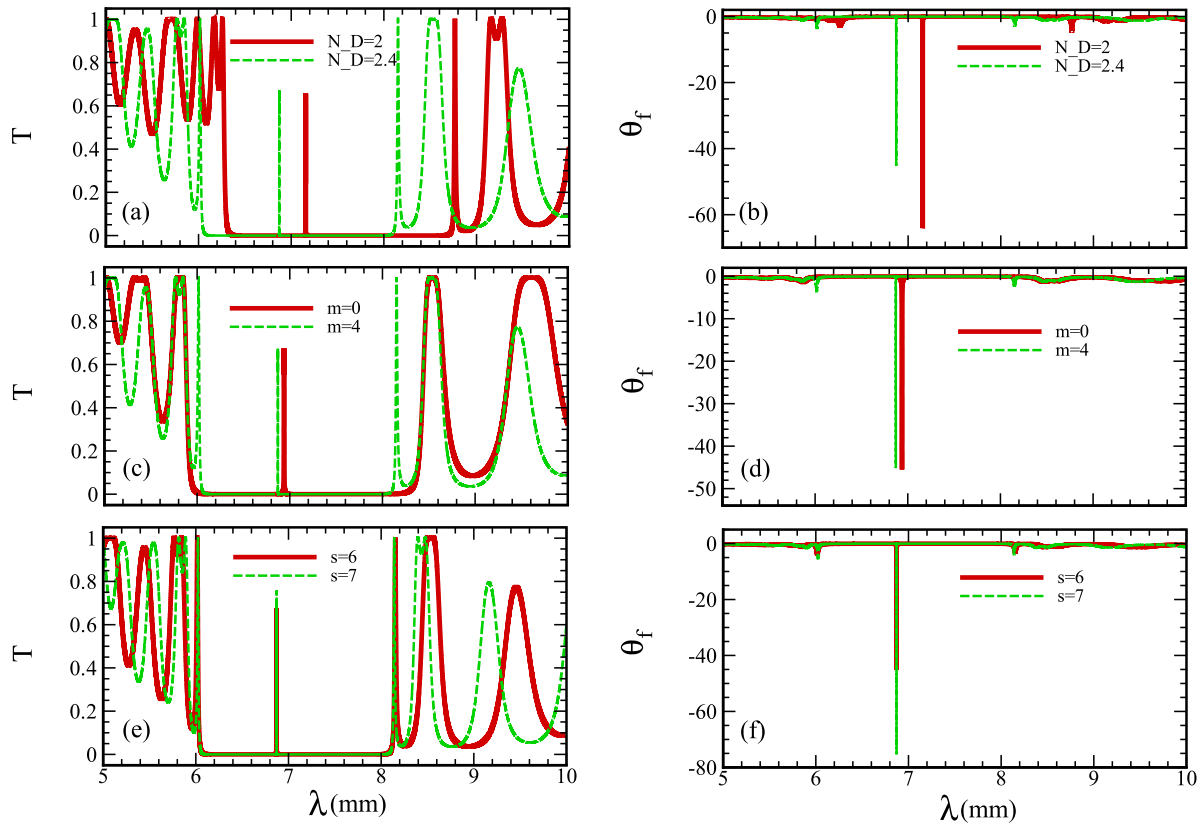

Figure 7. The transmittance and Faraday rotation angle for two different defect layer with different refractive indices ((a), (b)), for structure with defect and without defect layers ((c), (d)), and for two different s values ((e), (f)).

layers lie near together at the centre of the structure. The effects of change of repetition number of the surrounding unit cells on transmittance and Faraday rotation are presented in figures 7(e) and (f). They show that both Faraday rotation and transmittance increase when the number of surrendering layers increases.

It is worthwhile to discuss the novelty of our work and provide an outlook on the realization of the structure. In the structure considered here, plasma layers are used as one of the base layers of the photonic crystal. There are some research reports in the literature that use plasma systems as layers in photonic crystals [22–26], but tuning the Faraday rotation by magnetic field declination in the plasma photonic crystals have never been investigated. Therefore, investigating the tunability of Faraday rotation effect by magnetic field in a defected magnetized plasma photonic crystal is novelty of the current work. Also, the structure is completely novel because in this structure thickness of each dielectric layer is functioned by refractive indices of other dielectric layers. Unlike conventional magneto photonic crystals in which achieving high Faraday rotation in high transmittance is not feasible [9, 10], this structure tackles this problem and provides a high Faraday rotation in a high transmittance of the incident wave. Since the thickness of the plasma layer used in this work is not big (2.5 mm) creation of a uniform plasma with in this size range will not be a challenge in experimental applications. It can be established by using low-pressure argon glow discharge in which the discharge gap between parallel electrodes is divided into small volumes by dielectric layers normal to the surface of electrodes. The magnetic field can be applied by permanent magnets directed towards the sidewalls of the glow discharge reactor. This structure can be used for distinguishing, filtering, and isolation of CPs and have good potential in many applications, such as isolators, circulators, sensors, Faraday rotators, magneto-optical imaging [36–39]. In addition, it, due to its nonreciprocal properties, can be used to construct optical diodes that can transmit light in one direction and prevent its propagation in the reverse direction, as optical switchers [9].

4. Conclusion

A defected magnetised plasma photonic crystal has been considered to generate defect modes within generated photonic bandgap that could be used to directly analyse the effect of the variation of magnetic field declination on photonic crystals. The magnetisation of the plasma photonic crystal enables tunability of properties of the plasma layers, causing significant alteration of the transmittance, reflectance, and magneto-optical effects that arise when incident EM waves are propagating through the designed crystal. The generated resonance modes within the photonic crystal allow the Faraday rotation and ellipticity effects to be studied. The number of defect layers contributed significantly towards the positioning of defect modes within the photonic bandgap in addition to affecting the frequencies at which the resonant Faraday rotation and ellipticity effects occur, as well as the magnitude of these effects.

The transmittance and reflectance patterns obtained when varying the number of defect dielectric layers, which changes the total thickness of the defect layer, resulted in two defect modes within the photonic bandgap that began to converge from $m = 4$ to $m = 6$, but three defect modes were obtained for the photonic crystal where $m = 8$, resulting in an overlap of central defect mode of $m = 4$ and $m = 8$. The Faraday rotation and ellipticity responses displayed similar trends as those observed for transmittance and reflectance, with respect to the overlap observed for when $m = 4$ and $m = 8$, and the convergence of defect mode frequencies as m decreases. The transmittance and reflectance peaks occur at the same frequencies. A variation in the magnetic field strength changes the resonant frequency and magnitude for the defect modes. The Faraday rotation and ellipticity increased with increasing amplitude of external magnetic field. By changing the magnetic field declination angle, the resonant frequency values for transmittance can be altered with a very high levels of precision, whilst at the same time maintaining very similar peak Faraday rotation and ellipticity values. As the magnetic declination increased from 30° to 60°, the peak defect mode frequencies begin to converge, whilst the magnitude for these defect modes remains virtually the same. It was observed that the tunability of the resonance frequencies for transmittance and magneto-optical responses can become more and more precise when all of these variables are considered. The implications of these results with respect to potential applications are a significant improvement in photonic crystal-based waveguides and communications technology as signals can be received and sent with higher degrees of precision.

Data availability statement

The data that support the findings of this study are available from the corresponding author upon reasonable request.

Acknowledgments

N Pourali V, Hessel, and E Rebrov would like to thank the financial support from the ERC Synergy Grant 'Surface-Confined fast modulated plasma for process and energy intensification' (SCOPE) from the European Commission with the Grant No. 810182. Also, E Rebrov would like to thank the financial support from the Russian Science Foundation, (Project 20-69-46041) 'Intensification of dry reforming of methane on thin-film catalysts by forced periodic modulation of the electric field, concentrations and temperature distributions in a non-thermal plasma reactor'.

ORCID iDs

Nima Pourali https://orcid.org/0000-0002-0962-5926
Kevon Alexander https://orcid.org/0000-0002-0396-3756
Volker Hessel https://orcid.org/0000-0002-9494-1519
Evgeny V Rebrov https://orcid.org/0000-0001-6056-9520

References

[1] Van Vlack C, Kristensen P T and Hughes S 2012 *Phys. Rev.* B **85** 075303
[2] Yanik M F, Fan S and Soljačić M 2003 *Appl. Phys. Lett.* **83** 2739
[3] John S and Florescu M 2001 *J. Opt. A: Pure Appl. Opt.* **3** S103
[4] Weily A R, Esselle K P and Sanders B C 2003 *Phys. Rev.* E **68** 016609
[5] Upadhyay M, Awasthi S K, Shiveshwari L, Shukla S and Ojha S 2015 *J. Supercond. Novel Magn.* **28** 1937
[6] Upadhyay M, Awasthi S, Shiveshwari L, Shukla S and Ojha S 2016 *Indian J. Phys.* **90** 353
[7] Shukla S, Prasad S and Singh V 2015 *Phys. Plasmas* **22** 022122
[8] Zhang J, Zou J and Wang Y 2016 *Phys. Plasmas* **23** 102101
[9] Pourali N and Bahador H 2019 *Phys. Plasmas* **26** 013515
[10] Sattari M, Pourali N and Sadri B 2017 *J. Appl. Phys.* **122** 073102
[11] Sakai O, Sakaguchi T and Tachibana K 2005 *Appl. Phys. Lett.* **87** 241505
[12] Maigyte L and Staliunas K 2015 *Appl. Phys. Rev.* **2** 011102
[13] Qi L, Yang Z and Fu T 2012 *Phys. Plasmas* **19** 012509
[14] Inoue M, Uchida H, Nishimura K and Lim P B 2006 *J. Mater. Chem.* **16** 678
[15] Inoue M 2004 *MRS Online Proc. Libr. (OPL)* **853** 131–49
[16] Belotelov V *et al* 2011 *Nat. Nanotechnol.* **6** 370
[17] Pershan P 1967 *J. Appl. Phys.* **38** 1482
[18] Lyubchanskii I, Dadoenkova N, Lyubchanskii M, Shapovalov E, Zabolotin A, Lee Y and Rasing T 2006 *J. Appl. Phys.* **100** 096110
[19] Ardakani A G 2014 *J. Opt. Soc. Am.* B **31** 332
[20] Nishizawa H and Nakayama T 1997 *J. Phys. Soc. Japan* **66** 613
[21] Khanikaev A, Baryshev A, Inoue M, Granovsky A and Vinogradov A 2005 *Phys. Rev.* B **72** 035123
[22] Adamovich I *et al* 2017 *J. Phys. D: Appl. Phys.* **50** 323001
[23] Li Q, Hu L, Mao Q, Jiang H, Hu Z, Xie K and Wei Z 2018 *Opt. Commun.* **410** 431
[24] Yu G X, Fu J, Du W, Dong J and Luo M 2018 *Optik* **172** 401
[25] Awasthi S K, Panda R and Shiveshwari L 2017 *Phys. Plasmas* **24** 072111
[26] Hojo H and Mase A 2004 *J. Plasma Fusion Res.* **80** 89
[27] Goncharov A, Zatuagan A and Protsenko I 1993 *IEEE Trans. Plasma Sci.* **21** 578
[28] Dwyer T, Greig J, Murphy D, Perin J, Pechacek R and Raleigh M 1984 *IEEE Trans. Antennas Propag.* **32** 141
[29] Vidmar R J 1990 *IEEE Trans. Plasma Sci.* **18** 733
[30] Zhang H-F, Liu S-B and Kong X-K 2012 *Phys. Plasmas* **19** 122103
[31] Qi L, Yang Z, Lan F, Gao X and Shi Z 2010 *Phys. Plasmas* **17** 042501
[32] Kumar A, Khundrakpam P and Sharma P 2013 *AIP Conf. Proc.* **1536** 737–8
[33] Mehdian H, Mohammadzahery Z and Hasanbeigi A 2016 *Optik* **127** 3895
[34] Kahl S and Grishin A M 2005 *Phys. Rev.* B **71** 205110
[35] Višňovskỳ Š, Postava K and Yamaguchi T 2001 *Opt. Express* **9** 158
[36] Kato H, Matsushita T, Takayama A, Egawa M, Nishimura K and Inoue M 2003 *Opt. Commun.* **219** 271
[37] Śmigaj W, Romero-Vivas J, Gralak B, Magdenko L, Dagens B and Vanwolleghem M 2010 *Opt. Lett.* **35** 568
[38] Chung K, Kato T, Mito S, Takagi H and Inoue M 2010 *J. Appl. Phys.* **107** 09A930
[39] Sun T, Luo J, Xu P and Gao L 2011 *Phys. Lett.* A **375** 2185